Paper presented at 4th European Symp.
on Semiconductor Detectors, 3-5 March
1986, Münich, W. Germany; to be published
in Nucl. Instr. & Meth.

BNL--37899

DE86 009428

SILICON POSITION SENSITIVE DETECTORS FOR THE HELIOS (NA34) EXPERIMENT*

R. Beuttenmuller,[1] V. Bisi,[6] E. Chesi,[2] R. P. Di Nardo,[1] M. J. Esten,[3]
P. Giubellino,[6] H. W. Kraner,[1] T. W. Ludlam,[1] F. Meddi,[5] F. Piuz,[2] V. A.
Polychronakos,[1] V. Radeka,[1] L. Ramello,[6] R. Roosen,[4] and A. Tschulik[2]

March, 1986

[1] Brookhaven National Laboratory, Upton, NY 11973-5000 USA
[2] CERN, Geneva 23, Switzerland
[3] University College, London, United Kingdom
[4] Vrye Universiteit, Brussels, Belgium
[5] University of Rome, Italy
[6] University of Torino, Italy

---

*This research was supported by the U. S. Department of Energy under Contract No. DE-AC02-76CH00016 and by CERN, Geneva, Switzerland.

SILICON POSITION SENSITIVE DETECTORS FOR THE HELIOS (NA 34) EXPERIMENT*

R. H. Beuttenmuller,[1] V. Bisi,[6] E. Chesi,[2] R. P. Di Nardo,[1] M. J. Esten,[3] P. Giubellino,[6] H. W. Kraner,[1] T. W. Ludlam,[1] F. Meddi,[5] F. Piuz,[2] V. A. Polychronakos,[1] V. Radeka,[1] L. Ramello,[6] R. Roosen,[4] and A. Tschulik[2]

ABSTRACT

Silicon detectors having both "pad" and strip position sensitive configurations have been fabricated for the HELIOS experiment which requires an elaborate pulse height-dependent trigger as well as one dimensional silicon strip position sensing. The trigger detector is a 400 element, 30 mm diameter detector with readout connections from a ceramic overlay board. Tests with full prototype detectors have shown essentially 100% detection efficiency and excellent pulse height resolution well capable of delineating 0, 1 or 2 hits per pad. Strip detectors with 25 μm pitch and a varying readout pitch have been tested, which utilize both capacitive and resistive charge division. Techniques for realization of required inter-strip resistors will be discussed and results which may compare these readout methods will be reported.

*This research was supported in part by the U. S. Department of Energy under Contract No. DE-AC02-76CH00016 and by CERN, Geneva, Switzerland. By acceptance of this article, the publisher and/or recipient acknowledges the U. S. Government's right to retain a nonexclusive, royalty-free license in and to any copyright covering this paper.

[1] Brookhaven National Laboratory, Upton, New York 11973-5000, USA
[2] CERN, Geneva 23, SWITZERLAND
[3] University College, London, UNITED KINGDOM
[4] Vrye Universiteit, Brussels, BELGIUM
[5] University of Rome, ITALY
[6] University of Torino, ITALY

THE ROLE OF THE SILICON DETECTORS IN THE HELIOS EXPERIMENT

A brief outline of the experimental configuration of HELIOS will be helpful to suggest the design considerations and performance requirements of the silicon detectors. The experiment is a high precision measurement of lepton production in proton-nucleus collisions at the CERN Super Proton Synchrotron (SPS). HELIOS employs an electron spectrometer, a muon spectrometer, and an array of calorimeters for measurement of neutrinos and neutrino-like objects through missing energy and momentum, which are shown at the top of Fig. 1. The 450 GeV/c proton beam is especially designed to have a cross section of 30 μm in order to interact with a target which is a thin beryllium wire 50 μm in diameter and 2 cm long. The principal components of the electron spectrometer used for electron identification at the trigger level are a transition radiation detector consisting of polypropylene radiators viewed by a set of eight proportional chambers with an expected pion rejection of 2000 and a highly segmented uranium-liquid argon calorimeter. The calorimeter's electromagnetic front end is 20 radiation lengths with tower readout. Groups of towers are summed for an effective segmentation of 256 elements used by the trigger logic. An electron is identified by the coincidence of a signal from the transition radiation detector and energy deposition in a calorimeter segment consistent with an electron. This trigger is dominated by electrons produced in γ-conversions from π^0 decays.

The silicon "pad" detector, having an array of segmented collecting electrodes over an area with 30 mm diameter, is used to suppress this background in the following manner. The candidate electron trajectory is reconstructed using the information provided by hits in the calorimeter and the transition radiation detector (note the hits on the ray in the lower schematic), which are projected to the target. The Si pads surrounding the point at which this trajectory intersects the pad plane are then interrogated. For a proper electron one and only one particle should be observed. For an electron from a conversion, either two particles or none would be detected depending on whether the conversion took place before or after the Si pad detector. Monte Carlo simulations predict a suppression factor of 30 for conversions and a factor of 2 - 3 for Dalitz pairs due to the small opening angle of Dalitz electrons.

The considerations outlined in the previous paragraph led to the design of the detector shown in Fig. 2. The size of the pads reflect the expected secondary particle density, the smallest being 200 × 2000 μm. The pads are separated by 40 μm oxide boundaries which were found to be fully active. The dimensions of the pads in the two projections reflect the precision of the track extrapolation in these projections. Vertically the size is determined by the finite size of the target whereas horizontally the determining factor is the weak magnetic field which is ignored at the trigger level. The ≈.5 mm diameter hole in the center allows the unreacted beam through the detector.

The silicon strip detectors will provide some secondary vertex information for events which do pass the trigger condition. The tracking information is not required to be exhaustive or of specifically high spatial resolution.

THE PAD DETECTOR

Several series of pad detectors have been constructed from both n and p type high resistivity silicon. Silicon suppliers have been Komatsu and Wacker with 7 kΩ/cm n-type and 8 kΩ/cm p-type, 50 mm diameter (1,1,1) float zone refined silicon. Depletion of 300 μm occurs at ~40 and 120 volts, respectively, for these materials. The fabrication principles generally follow accepted industrial, oxide-passivated, "planar" technology, guided by the applications of Kemmer [1] to silicon detectors and with certain variations derived from experience in this laboratory. Generally, the process steps must be tailored towards simplicity and low temperature processes in order to preserve the lifetime and purity of high resistivity detector-grade silicon. Details of the fabrication technology which evolved for these detectors will be found in [2].

The pad pattern shown in Fig. 2 is boron implanted and the continuous back contact arsenic implanted, both at doses of 5×10^{14} ions/cm^2. The conventional configuration on n-type material depletes from the pads and operation of the devices at overvoltage, beyond depletion, is achieved. Leakage currents of even large pads are in the nanoampere range and they indicate that substantial minority carrier lifetime has been preserved through the processing. Several successful devices have also been made in p-type material which deplete into the pad pattern. Leakage current and capacitance versus applied bias are shown in Fig. 3 in which the precipitous drops at depletion are observed as the pad monitored takes on its single current and capacitance value, rather than that of the entire wafer area. A wide bias range above depletion is available for operation to assure complete depletion across the full device. The yield from this configuration was slightly higher than with the n-type substrate perhaps reflecting the advantage that the pad junction edges and corners are all at lower potentials and fields than they may be in the n-type base material configuration.

Figure 4 shows the finished detector as well as the individual pieces, the wafer and the ceramic motherboard. Contact is made to each pad by ultrasonic bonding with 25 μm Al-1% Si wire from the pad to bonding lands on the overlay board. All pads are at least partly exposed by the positions of the open slots; the intermediate fan-out from the bonding pads to the board edge can be seen. The ceramic board is 250 μm thick and was required because the number of leads on the interslot vias was sufficiently large to require lead pitches of ≈30 μ which are possible only on ceramic substrates. The metallization on the ceramic board is chromium. The slots were cut after the pattern lithography by a laser cutter; the board was supplied finished as shown by an outside firm. It was found that care had to be taken in the post-cutting anneal and that the slot ends should be well rounded to avoid thermal stress in corners and subsequent breakage.

After mounting and bonding to the ceramic board, the ceramic is in turn mounted on a larger G10 board, as shown in Fig. 4, which fans out to edge connectors on three sides having standard 2.5 mm pitch. The larger assembly is shown in Fig. 5, which includes the aluminum frame and support system and one preamplifier board inserted on the side. The back side of the wafer which is not obscured by the overlay boards is visible together with a bias filter and back pulser module. One small hybrid preamplifier [3] is shown inserted towards the bottom of the preamplifier board. The aluminum support frame is routed to reduce mass exposed to the scattered beam. To avoid crossing leads or signal paths and a multi-level board commitment, the preamplifiers (400) are all mounted peripherally with 0.1 inches required per preamplifier. Therefore 40 inches of periphery is needed which requires further fan-out from the G10 motherboard. An intermediate board is used between the motherboard and preamplifier board which is secured to an outer aluminum frame. This board provides the additional fan-out and mechanically isolates the detector board from the preamplifier boards and heavy cabling.

The lead capacitance from a silicon pad to the preamplifier is in the range of 20 pf which is the main source of series noise by the preamplifier. Whereas this value is obviously higher than one would like, it is acceptable for the purpose of this detector. Using a recent version of the Brookhaven hybrid preamplifier with bipolar shaping amplifiers with 200 nsec peaking time, noise levels of equivalent noise charge of 500 electrons (σ) are observed.

PAD DETECTOR TESTS

Two requirements of the pad detectors were tested with minimum ionizing particles: 1) that the device have adequate energy resolution of events to permit delineation of single or double hits per pad (or none) and 2) that the detector have high overall efficiency, including as much as possible of the interpad regions covered by oxide. In practice for each pad hit and interrogated for a valid trigger the adjacent pads are also summed in pulse height information and it is the sum which should unequivocally produce a 0, 1, or 2 hit decision. Nevertheless if charge is lost from events in the interpad region, a trigger decision could be compromised.

The detectors were tested at the CERN Proton Synchrotron (PS) and Super Proton Synchrotron (SPS) using similar setups. Figure 6 shows the device set-up at the SPS. A 200 Gev/c pion beam is defined by a high resolution tracking telescope consisting of 14 planes of micro-strip detectors. These planes were arranged in seven pairs each with one detector with readout in the x directon and another with readouts in the y direction. Each plane consisted of 192 strips with 50 μm pitch. An independent trigger was provided by two small (1 × 1 cm) scintillators. The detector under test (shown in Fig. 5, e.g.) was mounted on a micrometer x-y stage so that the entire active area could be sequentially illuminated.

A composite of the pulse height distributions from several of the smaller pads produced a fit to a Landau distribution with the most probable loss of 79 ± 2 keV with $\sigma = 6.9 \pm 0.5$ keV in good agreement with the results of others [4]. The absolute energy scale was determined by injecting a known amount of charge through a calibration capacitance. In addition to determining the overall detector efficiency, a thorough understanding of the behavior of the detector near the pad boundaries is also essential in order to properly set the discriminator thresholds to detect one or two minimum ionizing particles. The microstrip detector telescope shown in Fig. 6 provides an ideal tool to study these edge effects as specific particle trajectories can be selected with high spatial resolution. The trajectories of beam particles triggering the system were reconstructed off-line using the microstrip detector information and unambiguous single tracks were selected and projected at the plane of the detector. The error on the position of the intersection point at the pad detector was found by plotting residuals to be 20 μm for the SPS test. Fig. 6 (lower) defines two areas A and B, both 1 mm x 100 μm, in the central area of a small pad and at the boundary with an adjacent pad, respectively. The pulse height distribution for those tracks which traverse the detector through A is shown in Fig. 7. It should be noted that no pedestal subtraction was performed on these pulse heights. When a pulse height "cut" for all events above one third of the most probable value of the energy loss is taken, 98% of all events are included. This efficiency represents only a lower limit of the full pad efficiency, however, as some of the events with pulse heights below the cut share their charge with a neighboring pad, but were incorrectly selected because of the finite resolution of the telescope.

Figure 8 shows the pulse height distribution for events selected to be in area B in the boundary of two adjacent pads. The upper two graphs in Fig. 8 show the pulse height distributions from the two pads and the third displays the distribution of the sum of the energy loss in each pad from this set of events. The sum distribution clearly shows that no events are lost traversing the boundaries of two neighboring pads because no events are seen in the low energy tail of the distribution. Therefore, the measured absolute detection efficiency for this pair of pads is 100%. Obviously the spatial reconstruction uncertainty is less important in this case. An error of two standard deviations would still place an event well within the region where the full charge is collected in one pad. The pulse heights of events selected in this manner can also be used to further determine the region about the boundaries where a given event contributes to the pulse heights of both pads. Figure 9 shows the mean pulse height as a function of position across the pad normalized to the pulse height in the center of the pad. It can be seen that charge sharing occurs in an area of, at most, 20 m from the boundary, and 20 m was the telescope position resolution. The true charge sharing region is estimated to extend 10 m on either side of a boundary with charge diffusion providing the main contribution (10 m for 300 m thick wafer and typical drift fields of 1 kV/cm). Less important is the beam divergence (15 mrad FWHM) which could cause a track to cross the cells of two adjacent pads if the point of incidence was within 3 m from the boundary.

Most of the 400 pads were studied in this manner. About eight pads did not function at all due to high leakage current. The overall detection efficiency of the remainder of the detector was greater than 98%. An event was considered detected if the collected charge on any pad was greater than one third of the charge expected for a minimum ionizing particle. Some of the nonfunctioning pads have the charge deposited in them collected by a neighboring pad. This phenomenon (observed also by others working with silicon detectors [5]) is probably due to open wire bonds which allow the potential of the pad to float to some value below the bias potential instead of being at virtual ground and charge is therefore more directly collected by a neighbor.

STRIP DETECTORS

The strip detectors shown in Fig. 1 have their 25 μm pitch strips in the vertical direction and are roughly segmented to increase granularity in the central region by division into an upper and lower central group. Each of the four subdivisions in each detector uses 100 readout channels for the 200, 400, and 600 strips in each subdivision starting from detector 1 through 3. Therefore detector 1 uses one intermediate strip (not read out) between readout channels, detector 2 has three intermediatestrips and detector 3 has five intermediate strips. Interpolative readouts will therefore be required which fall into two categories: capacitive and resistive charge division, illustrated in the schematic of Fig. 10. Capacitors C_2 are the strip-to-ground capacities which are ≈0.1 pf/cm for 25 μm pitch cells, 300 μm thick. C_1 are the interstrip capacities which are ≈1 pf/cm and the resistors R are externally added across the strip pattern. In early work, some resistance was found to be required to prevent strips between readouts from charging to a lower potential than the low impedance readout strips and altering the internal collecting field [6].

It is convenient and prudent with regard to noise considerations to add very large values of R, ≈10 MΩ, which generally assures capacitive charge division that has been well studied by Kötz et al. [7]) and Belau et al. [8]. Charge division can be characterized as either resistive or capacitive if the combined RC product is much greater than τ (capacitive) or is less than or of the order of the amplifier shaping time constant τ (resistive). The time constant of interest is approximately the total interstrip resistance between readout channels (ΣR) times the sum of the intermediate strip capacities from strip to ground (ΣC_2). For a test detector that will be described with strips of 25 μm pitch, 1.5 cm long with three intermediate strips per readout, if R is 2 MΩ and C_2 is .15 pf, ΣR•ΣC is 3.2 μsec. Although this is very long compared to 250 nsec shaping amplifiers used with high energy test beams, it is approaching the longer shaping times available in slower laboratory amplifiers (≈2 μsec).

A test detector with 400 strips with 25 μm pitch, 1.5 cm long, was divided into four groups of 100 strips each, such that every strip of the first group was read out, and every other in the second group, every third in the third group and every fourth in the fourth group were read out. Thus the strip detectors 1 and 2 are simulated. These detectors were conventional 300 μm thick, n-type planar devices with B implanted (p^+) strips and As implanted n^+ back contact. A resistive layer was applied across all the strips by the vacuum evaporation of germanium through an evaporation mask which could be varied in width between 50 μm and several millimeters. Evaporated germanium might be expected to achieve the bulk resistivity of 50 Ω cm in thickness over 1000Å, so that a "witness" sample that measures the resistivity per square during the evaporation would be an accurate measure of the interstrip resistance achieved in the detector. A direct, linear relationship between the witness sheet resistance and the interstrip resistance has not thus far been observed so that a more empirical procedure based on experience with previous evaporations and subsequent interstrip R measurement is used. Resistances down to 1.6 MΩ have been produced and it is expected that values into the 100 KΩ range can be achieved with this straightforward technique. Interstrip resistances are measured by observing the dc current at several low voltages between one strip and its adjacent neighbors together and must be made with the detector to some degree depleted. As observed by Klanner [9], a clear increase in the interstrip current occurs at ≈ ± 8V as injection from one p^+ contact into the other is possible after a small potential barrier created by interstrip surface charge is overcome. The value of interstrip resistance assumed from the dc i–v measurement is the small signal value between ± 2 volts.

Charge fractions from the several strip configurations were measured for several test detectors with 10 GeV minimum ionizing particles in the test beam at the CERN Proton Synchrotron. Although it was hoped that test devices would be available with interstrip resistance less than 1 MΩ, to approach resistive charge division, only one run with $R \approx 10$ MΩ, capacitive, was instructive. The test detector was placed between the first two planes of a three unit 50 μm pitch strip detector telescope with each plane separated by ≈20 cm. Analysis of residuals between the telescope planes yielded a $\sigma_y \approx 20$ μm which is adequate to position events on particular strips between readouts.

Figure 11 (top) plots the ratio of charge collected on one readout channel to the sum of charge collected on that channel and its nearest neighbor (PH1/PH1+PH2) versus the position of the traversing particle between the two readout channels. The data are the composite from five instrumented readout channels of a test detector with 10 MΩ interstrip resistance in the area with three intermediate strips between readouts and are selected from events which are registered on only two adjacent strips. A nearly linear relation between the outputs of the adjacent 100 μm spaced readout channels is apparent, with the y axis data spread containing the Landau distribution from each event and the x axis fluctuations due to the telescope uncertainty. Figure 11 (lower) is the y-projection of Fig. 11 (top) which plots the number of events versus the observed collected charge fraction PH1/PH1+PH2. Three clear charge groups are found due to each of the three intermediate strips. The position of each charge fraction is at ≈.25, .5, and .75 of the sum does not suggest resistive charge division as the sum. When the collected charge sum, PH1 + PH2 is plotted versus the predicted particle position, a definite "sag" or decrement in total collected charge is found for the central strips compared with events hitting the readout strips as has been observed by Kötz et al.[7]. This indicates that the charge division is capacitive and not resistive, as one would expect from the consideration of the time constants discussed previously. This deficit in collected charge and the capacitive coupling (crosstalk) across several readout channels which may reduce two-track resolution beyond that of the strip pitch are the two problems with capacitive division which resistive division is intended to mitigate.

We are indebted to Robert Klanner, DESY, for the suggestion that alpha particles are a useful laboratory-scale source of events in strip detectors for tests of charge division. A ^{241}Am source has been used as a source of short-ranged charge deposition (20 μm range) in test strip detectors with interstrip resistances down to 1.6 MΩ. A simple readout and data analysis mode is provided by a standard two dimensional pulse height analyzer (Nuclear Data ND76) with the outputs of two adjacent readout strips connected to each ADC (data axis). Figure 12 shows a run with alphas incident on the strip side of the detector used previously with minimum ionizing particles with capacitive charge division: the lower figure rotates the axes into the plane of the paper and illuminates channels having more than 150 counts. A definite decrement in collected charge is noted for the intermediate strips as should be expected for the capacitive charge division. Figure 13 shows similar data for a test detector with 2 MΩ interstrip but with the amplifier filter time constants varied between 0.5 and 1.0 sec in an effort to demonstrate a marginally resistive charge division even with a high interstrip resistance. In both cases, a lower charge loss in central strips is observed.

One observation can be reported that is of peripheral interest in using an alpha source for charge division measurements. When alphas were introduced into the back contact, absolutely featureless linear distribution of shared charge between adjacent contacts at a somewhat reduced sum value was observed. Although depletion occurred from the strip to the back contact, the detector operated with over voltage and only a small effect of diffusion (10 m) might be expected even for charge traversing essentially the entire detector thickness, compared to an average thickness value when using particles which deposit energy uniformly across the detector. An explanation for the very uniform charge sharing however does suggest that a much larger component of diffusion than expected was present to spread charge over several strips. This explanation was confirmed by the fact that collected charge from each event was indeed found over three (or more) adjacent strips. Calculations by England [10] and Gatti [11] have shown a major effect of mutual repulsion of charge when deposited charge densities are large (10 carriers/20 m) which augments and surpasses diffusion giving charge spread over ≥ 150 m for a 300 m detector. This effect may well have caused the large charge spread over several readout channels.

SUMMARY

Silicon detectors are used in the HELIOS experiment for both tracking and vertex recognition and as an essential element on the electron trigger. A 400 unit large area "pad" detector has been built with planar technology and successfully operated in the electron trigger configuration during the initial summer running period, 1985. The active area of the device proved to be 97% of the 30 mm diameter device and tests with a beam telescope showed essentially no inactive regions between adjacent pads. Devices with p^+ boron implants in the pads and arsenic n^+ implants on the back wire built on n or p type material which deplete from either the pads or the back into the pads. The latter configuration may have certain production advantages.

To anticipate the charge division requirements of the strip detectors for HELIOS, a test strip detector has been constructed with several members of intermediate strips between readout channel strips. A resistive strip of vacuum-evaporated germanium provides interstrip resistances approaching values low enough for which resistive charge division can be expected. Tests with 10 GeV minimum ionizing particles at the CERN PS have demonstrated the capacitive charge division for the strip detectors with higher values of interstrip resistance as expected. Laboratory tests with alpha particles have demonstrated the linear resistive charge division at an appropriate value of the time constant formed by interstrip resistance R and strip-to-ground capacitance in relation to the amplifier shaping time.

ACKNOWLEDGEMENTS

We thank Graham Smith for sharing with us the two dimensional pulse height analyzer. The considerable mechanical skills of T. D. Williams, CERN, enabled precise alignment of the strip detectors in the test beams and are gratefully acknowledged. Several helpful discussions with Robert Klanner, DESY, in addition to his suggestion of the alpha source were very much appreciated.

BIBLIOGRAPHY

1. J. Kemmer, Nucl. Instr. & Meth. 169 (1980) 449.
2. R. Beuttenmuller *et al.*, IEEE Trans. Nuc. Sci. NS-33 (1986) No. 2.
3. We are indebted to D. Stephani, BNL, for developing and supplying the hybrid preamplifiers. The preamplifiers can be obtained from Rel Labs, Plainview, LI, NY.
4. S. Hancock *et al.*, Phys. Rev. A28 (1983) 615.
5. E. Heijne, CERN, personal communication and W. R. Th. Ten Kate, Delft, this conference.
6. B. Hyams *et al.*, Nucl. Instr. & Meth. 205 (1983) 99.
7. U. Kötz *et al.*, Max Planck Institute Report, Münich, MPI-PAE/Exp. El 142, November, 1984.
8. E. Belau *et al.*, Nucl. Instr. & Meth. 214 (1983) 253.
9. R. Klanner *et al.*, this conference.
10. J.B.A. England *et al.*, Nucl. Instr. & Meth. 185 (1981) 43.
11. E. Gatti, this conference.

FIGURE CAPTIONS

Fig. 1. Schematic arrangement of detectors in the HELIOS experiment. The silicon pad and strip detectors are enlarged in the lower portion.

Fig. 2. The pad detector layout. The active diameter is 30 mm.

Fig. 3. The leakage current and capacitance as a function of detector bias for the pad detector based on p-type material. As suggested by the inset, the active junction is the arsenic implanted back contact from which depletion occurs.

Fig. 4. The pad detector wafer (lower right) along with the ceramic overlay (lower left) and the G10 motherboard assembly.

Fig. 5. The pad detector assembly viewed from the back contact showing the intermediate boards and one preamplifier board.

Fig. 6. Schematic of pad detector tests at the SPS showing strip detector telescope system (upper portion) used to select events in each region (A and B) of adjacent small pads (below).

Fig. 7. Energy loss distribution for events selected to cross region A.

Fig. 8. Energy loss distribution for two adjacent pads for events in area B (upper two histograms) and the distribution of the sum of the two pulse heights (lower histogram).

Fig. 9. The mean energy loss (pulse height) as a function of position across a pad normalized to the energy loss in the center of the pad.

Fig. 10. Schematic of strip detector resistances and capacitances relevant to resistive and capacitive charge division.

Fig. 11. The charge collected on one readout strip divided by the sum of the collected charge on that strip and its neighbor versus predicted particle position for the strip test detector in the 10 GeV PS particle beam (upper portion). This data is from the area with three intermediate strips. In the lower portion, number of events versus pulse height fraction are plotted. This is the y-projection of the data above.

Fig. 12. Charge division between adjacent readout strips of the test detector with three floating strips and interstrip resistance ≈ 10 MΩ. Each readout strip is one horizontal axis on the display and shared charge puts events in the horizontal plane. The lower figure is the display of the horizontal plane with strip axes vertical and horizontal, the origin being the lower right corner. A ^{241}Am alpha source was used in the laboratory.

Fig. 13. Two dimensional display of alpha source on a test strip detector having three intermediate strips between readout channels. A lower interstrip resistance was present in the case, 1.6 MΩ and the results with two amplifier time constants are shown.

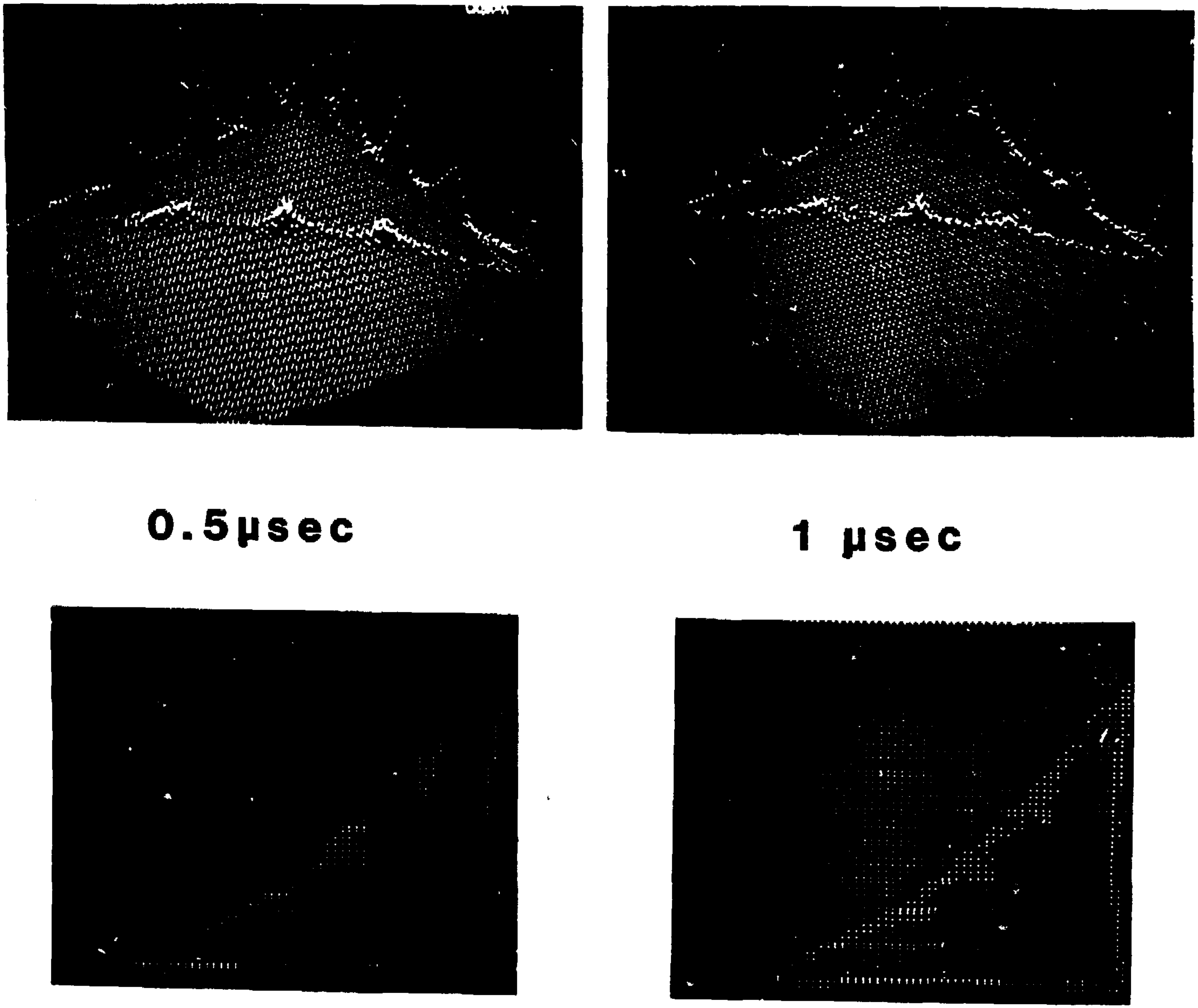

0.5µsec

1 µsec

Fig. 13

HELIOS (NA 34)

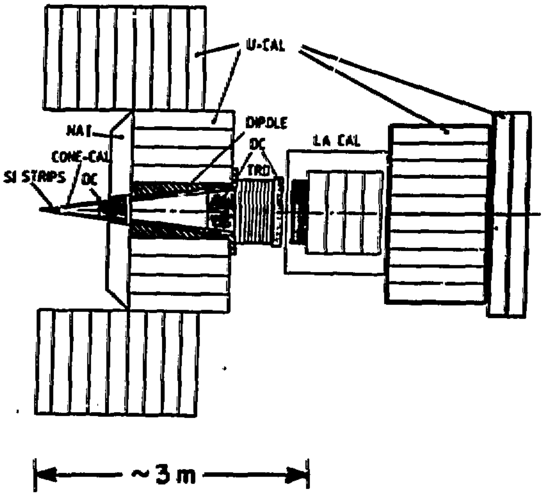

SILICON STRIPS

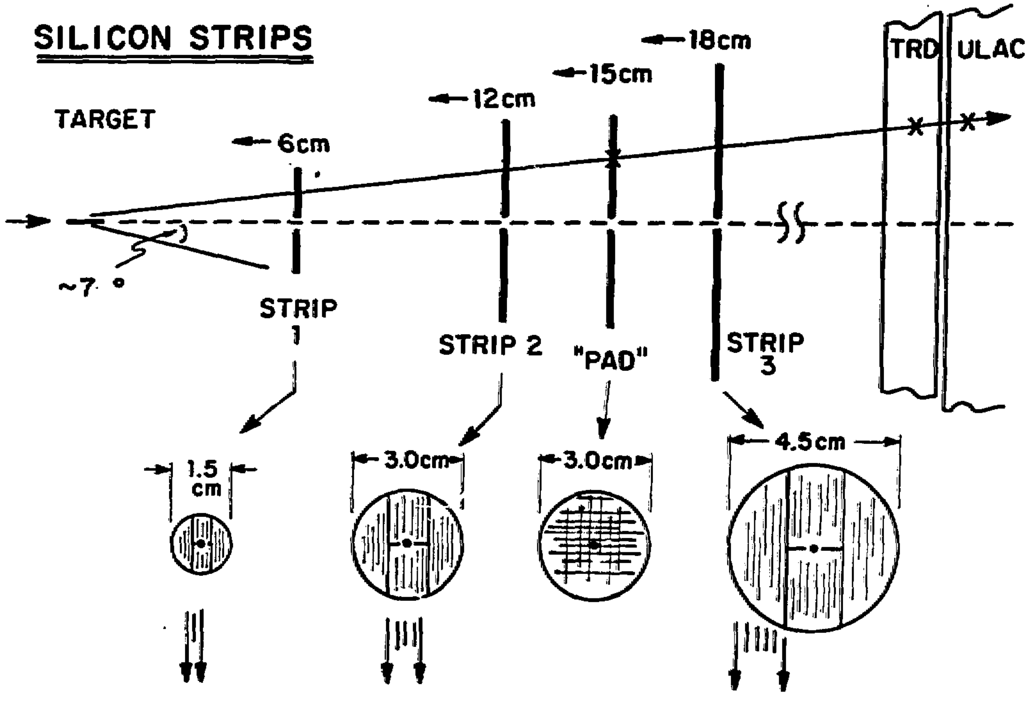

Fig. 1

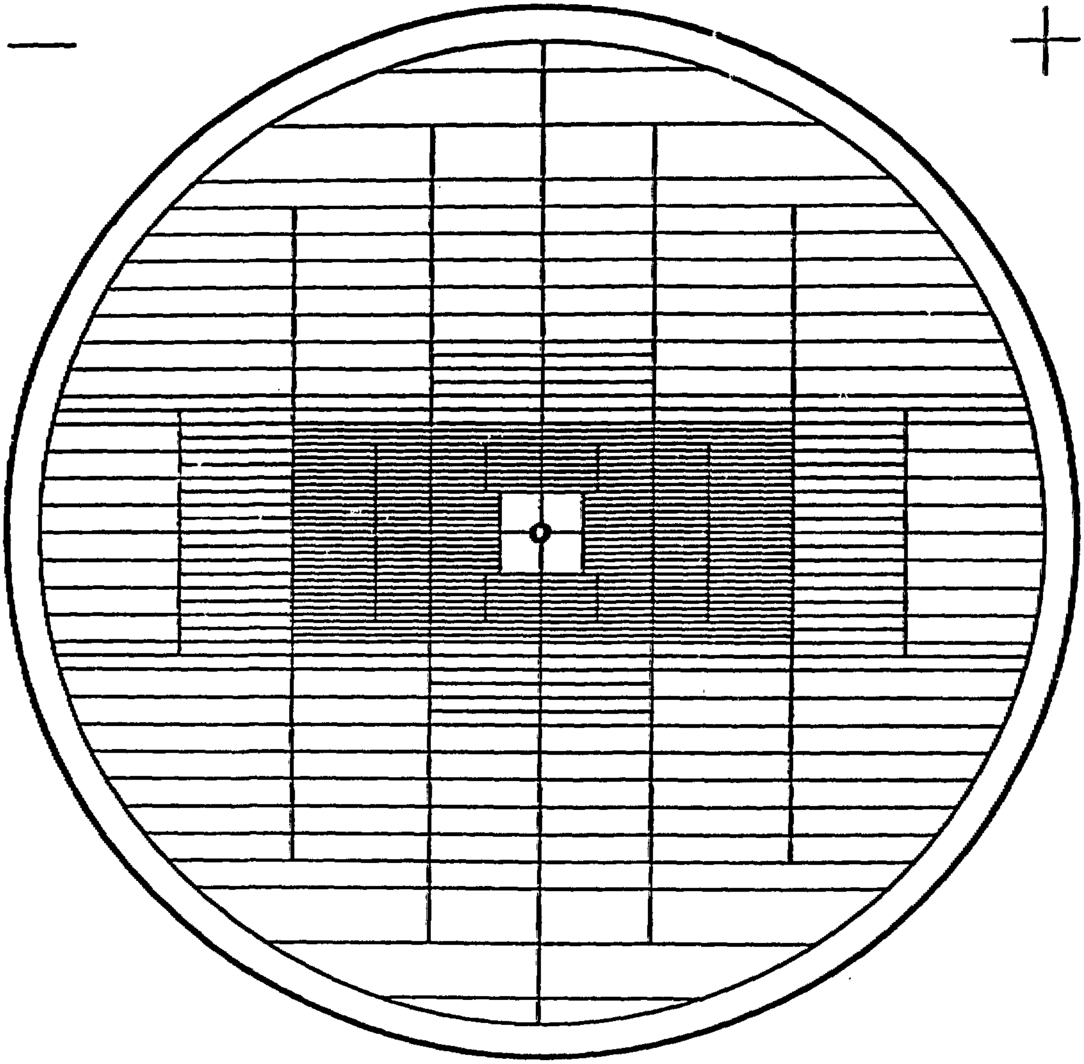

Fig. 2

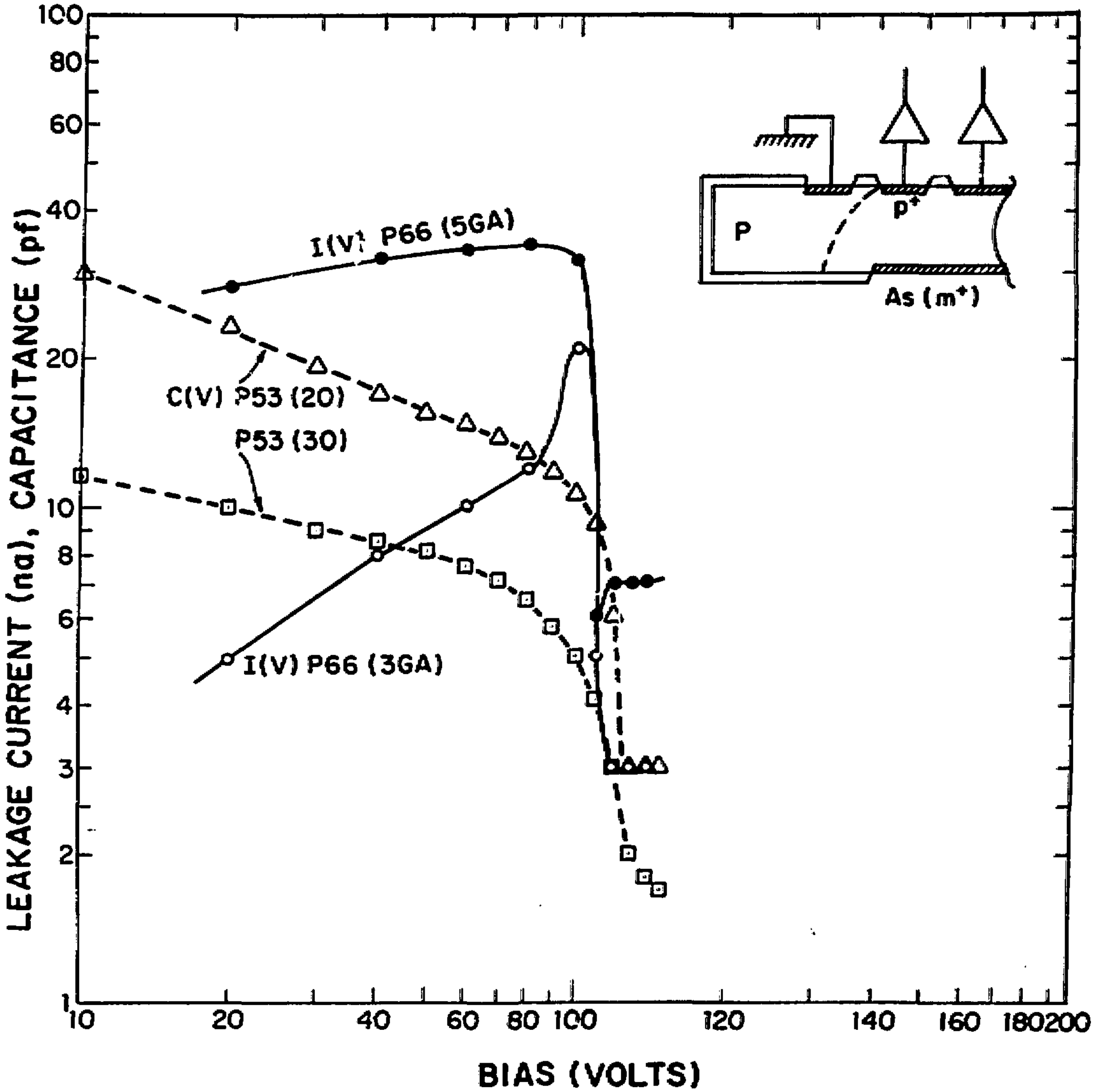

I(V) P66 (5GA)
C(V) P53 (20)
P53 (30)
I(V) P66 (3GA)
P
p+
As (m+)
LEAKAGE CURRENT (na), CAPACITANCE (pf)
BIAS (VOLTS)
1
2
3
4
6
8
10
20
40
60
80
100
10
20
40
60
80
100
120
140
160
180200

Fig. 3

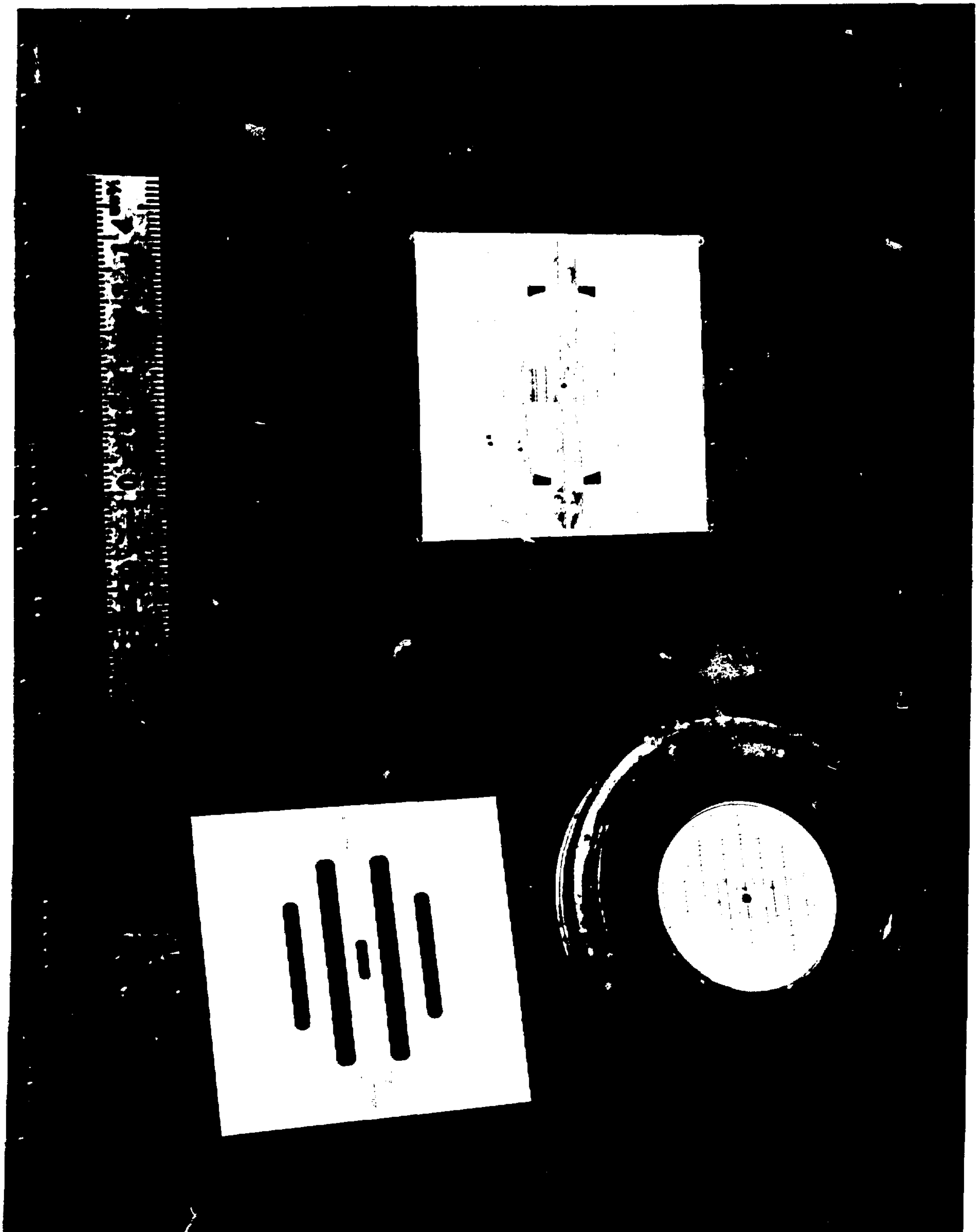

Fig. 4

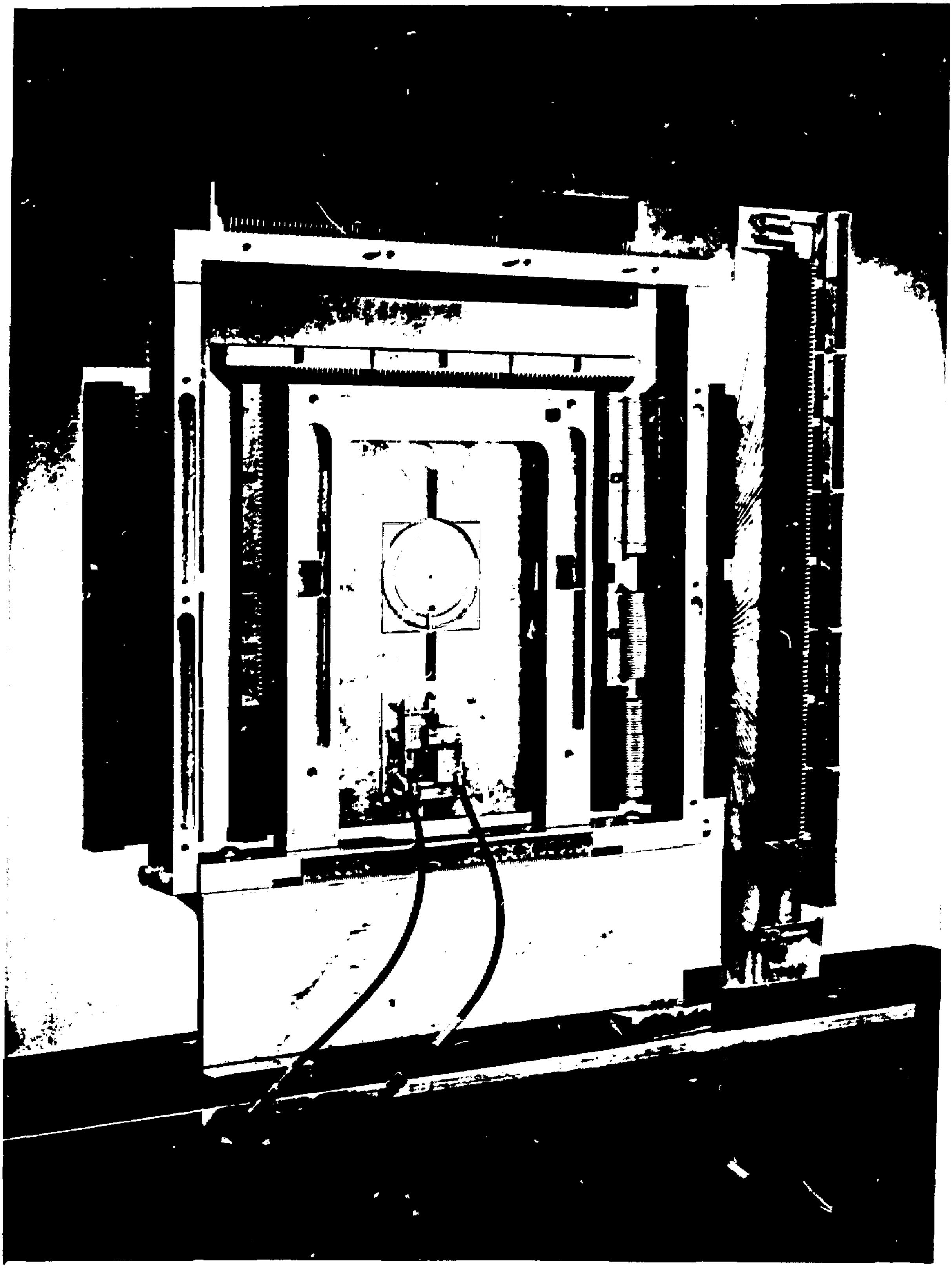

Fig. 5

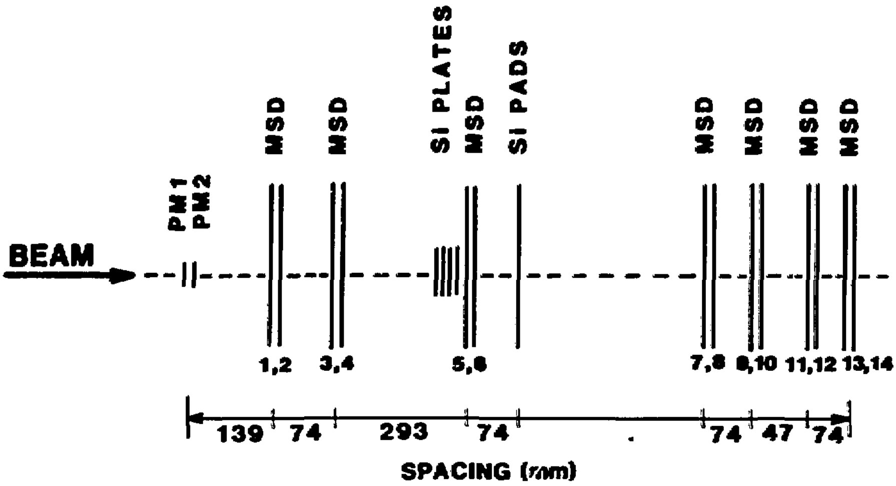

TRIGGER: PM1·PM2·SI PLATES

MSD: 192 STRIPS, 50μm PITCH

RESOLUTION OF MSD TELESCOPE: 20μm (σ)

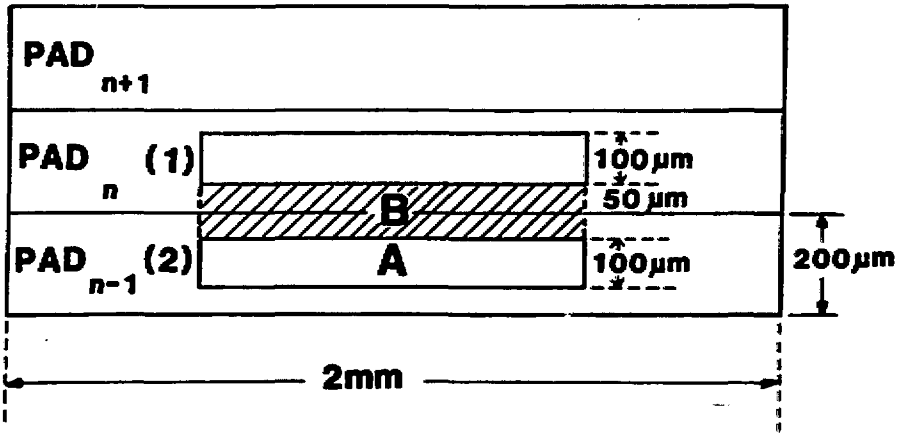

Fig. 6

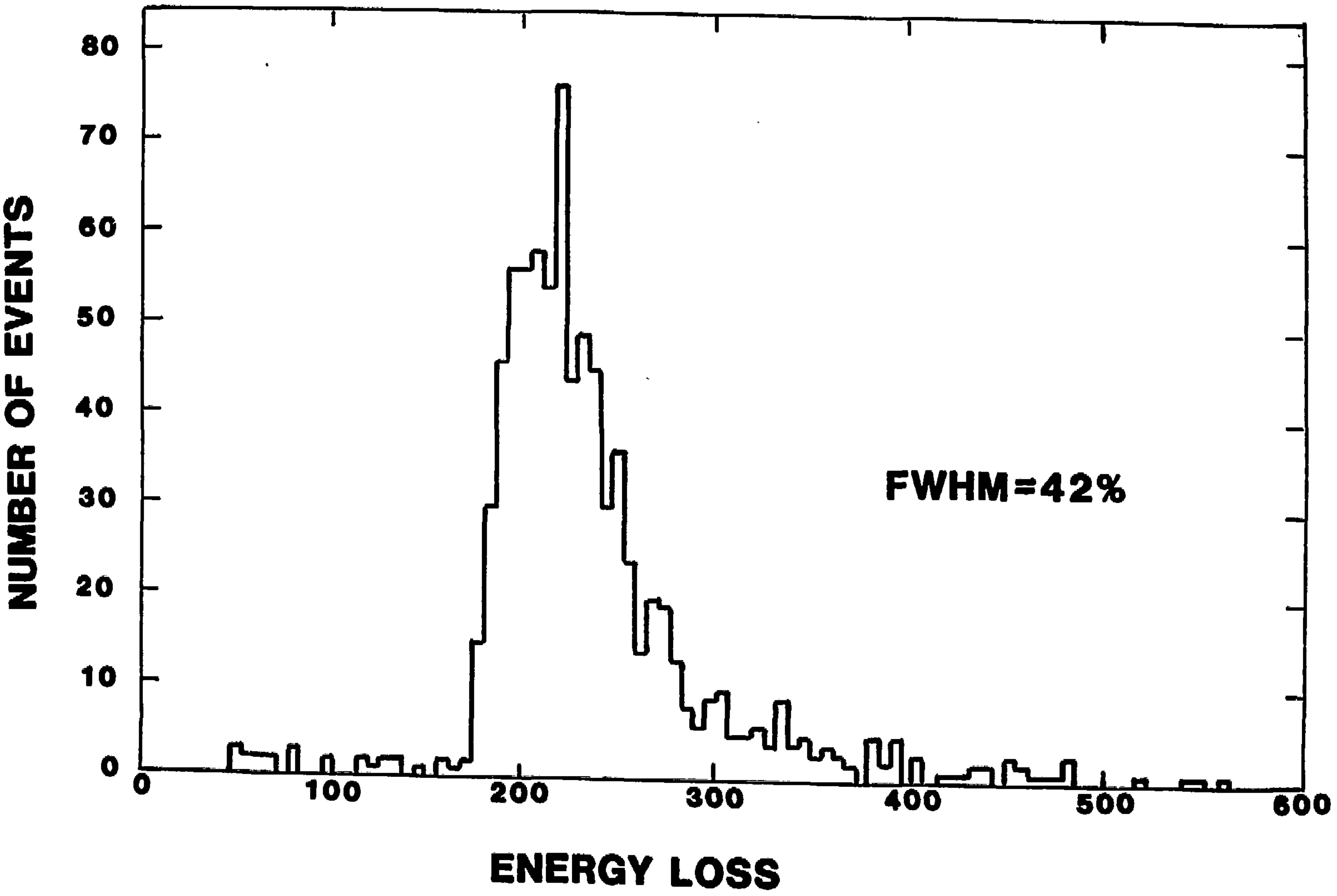
NUMBER OF EVENTS
0
10
20
30
40
50
60
70
80
0
100
200
300
400
500
600
ENERGY LOSS
FWHM=42%

Fig. 7

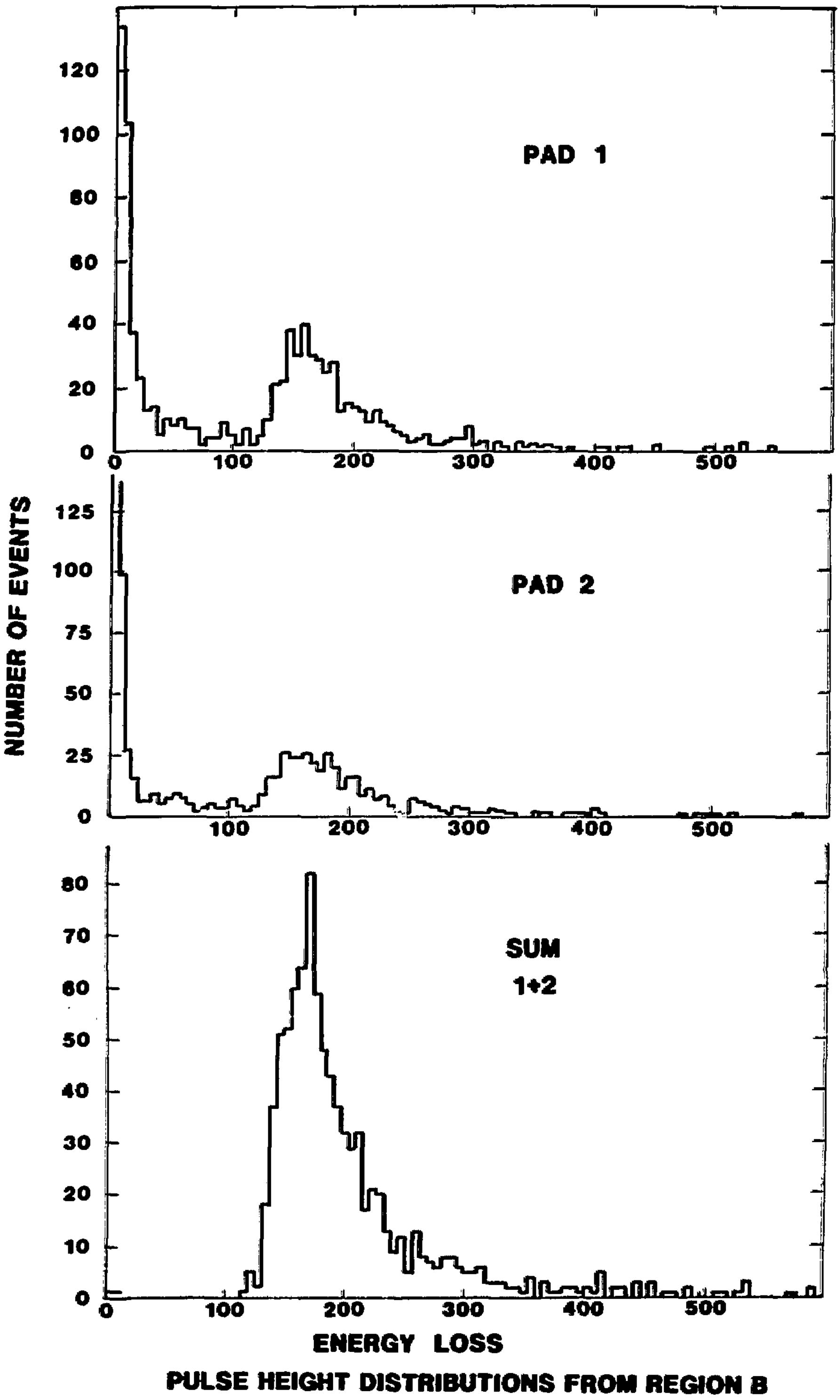
PAD 1
120
100
80
60
40
20
0
0
100
200
300
400
500
NUMBER OF EVENTS
PAD 2
125
100
75
50
25
0
100
200
300
400
500
SUM
1+2
80
70
60
50
40
30
20
10
0
0
100
200
300
400
500
ENERGY LOSS
PULSE HEIGHT DISTRIBUTIONS FROM REGION B

Fig. 8

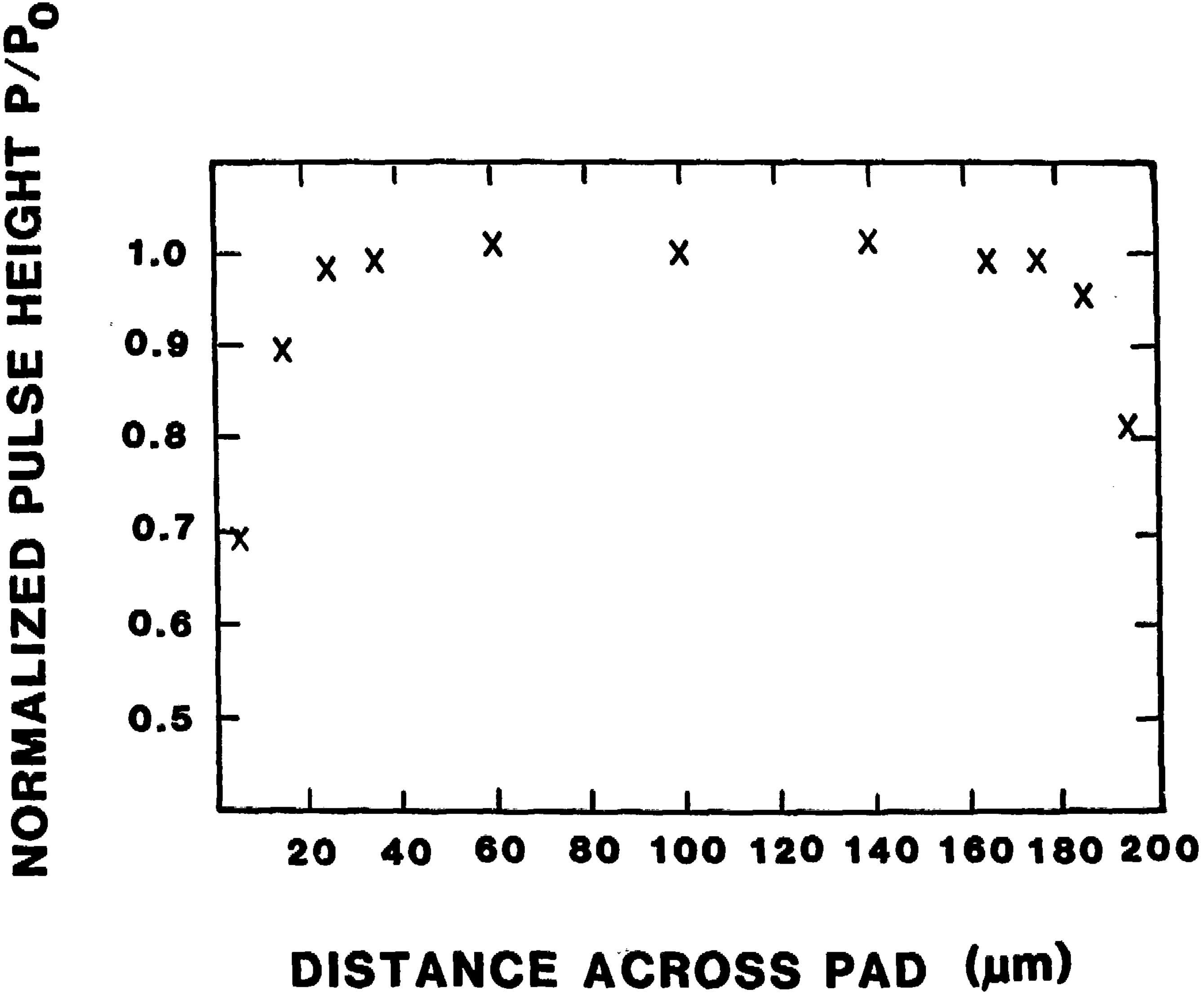
NORMALIZED PULSE HEIGHT P/P_0
1.0
0.9
0.8
0.7
0.6
0.5
20
40
60
80
100
120
140
160
180
200
DISTANCE ACROSS PAD (µm)

Fig. 9

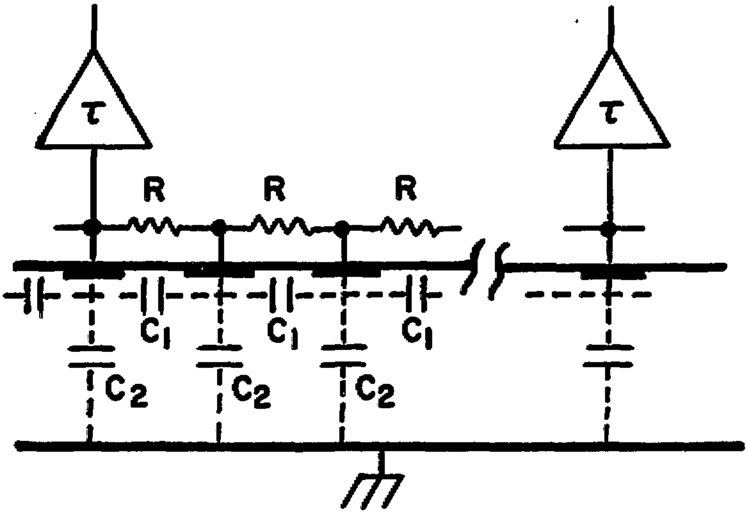

Fig. 10

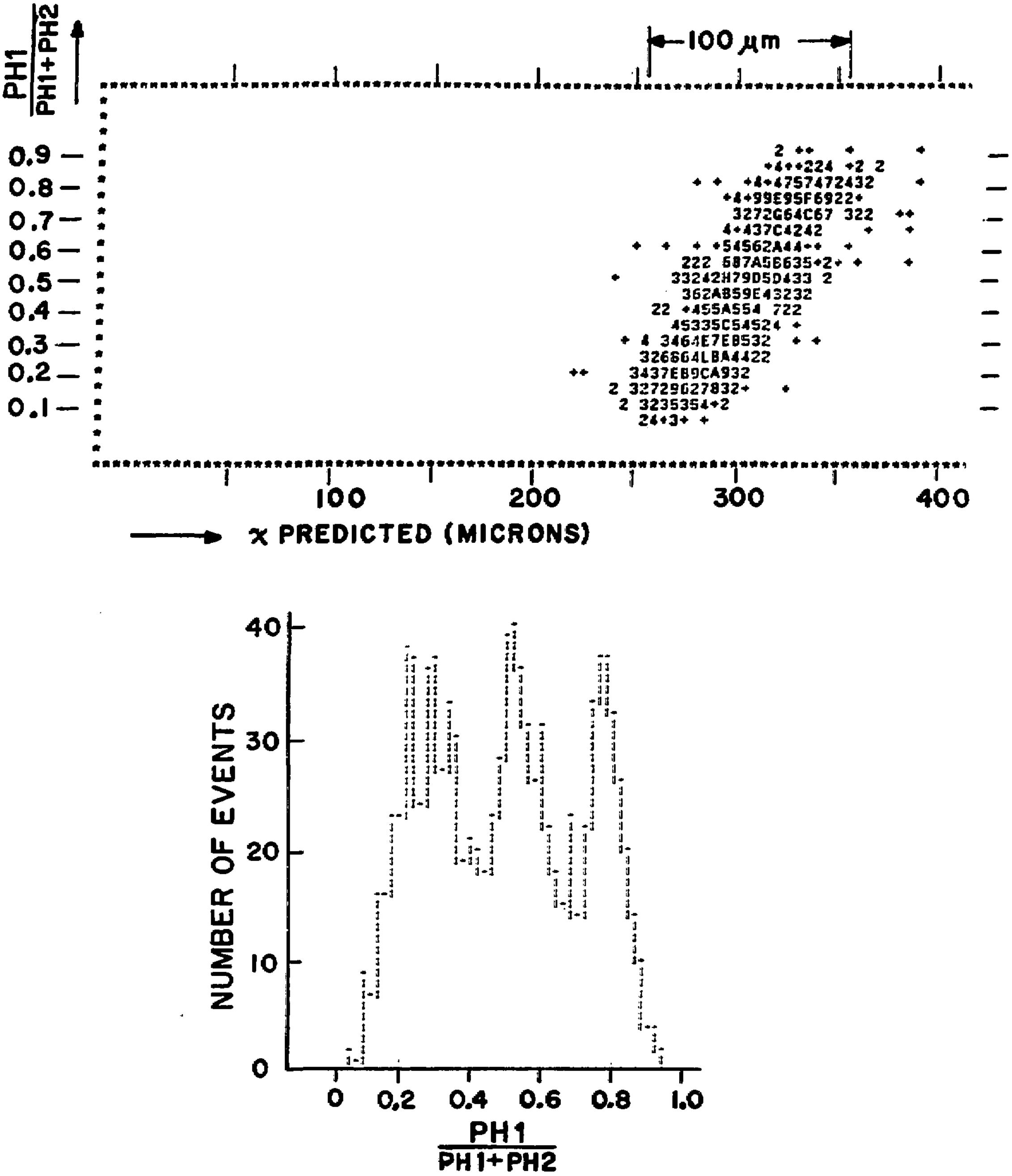
PH1/(PH1+PH2)
100 µm
0.9
0.8
0.7
0.6
0.5
0.4
0.3
0.2
0.1
100
200
300
400
x PREDICTED (MICRONS)
NUMBER OF EVENTS
40
30
20
10
0
0
0.2
0.4
0.6
0.8
1.0
PH1/(PH1+PH2)

Fig. 11

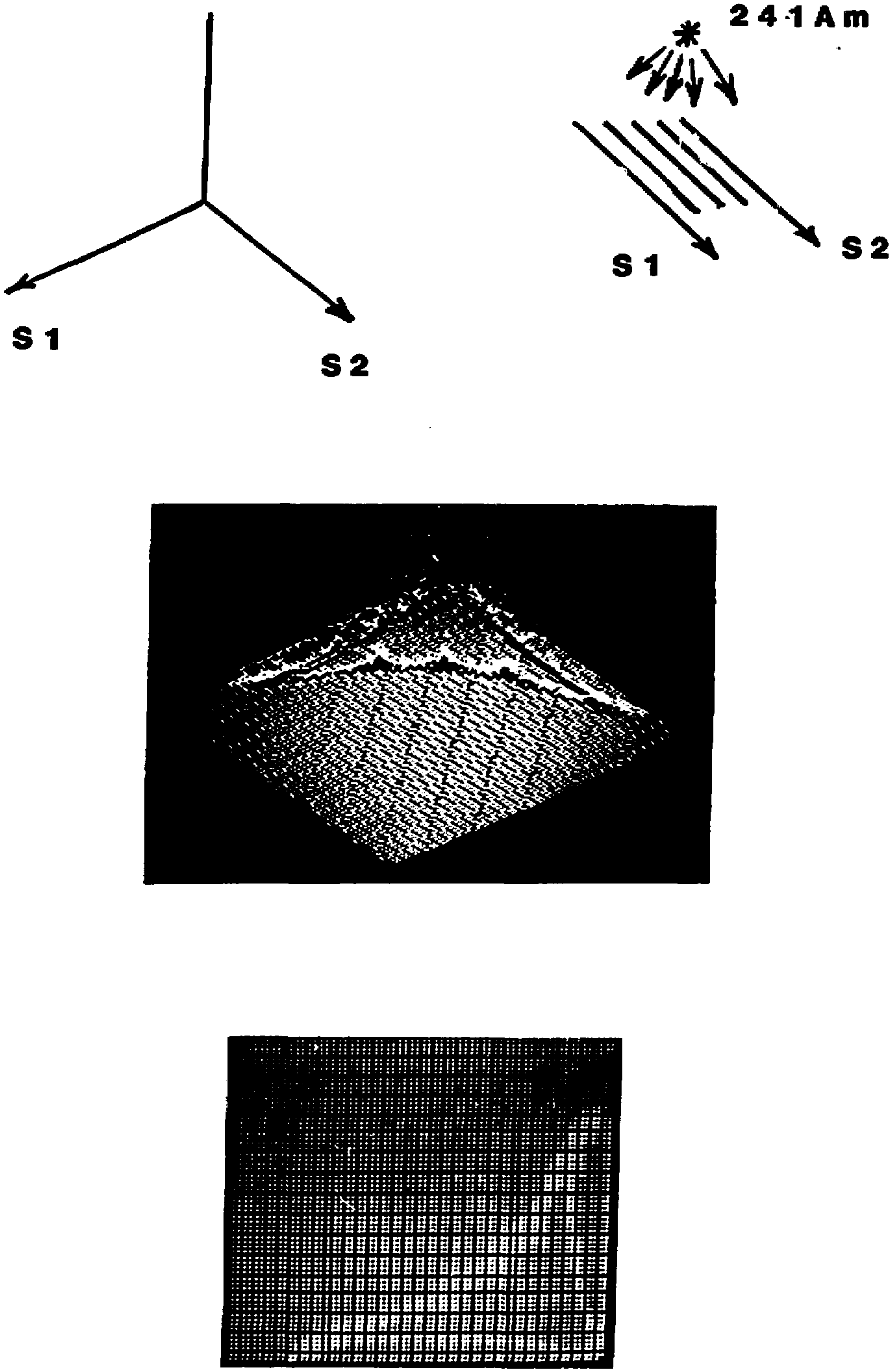

Fig. 12